3D Topology of Transient Bifurcation Just Before Substorm Onset

Peikun Xiong, Shigeru Fujita, Masakazu Watanabe, Takashi Tanaka, and Dongsheng Cai

Abstract – In this study, we report a transient bifurcation just before the substorm onset, occurring in the three-dimensional topology of Earth's magnetosphere from a global Magnetohydrodynamics simulation when the interplanetary magnetic field (IMF) has a non-zero east-west component. Using the geodesic level set method, we extract two-dimensional separatrices from magnetic nulls near Earth's poles. Our visualizations reveal critical saddle-connected manifolds on both the dusk and dawn sides of the magnetosphere. On the dusk side magnetotail, the neutral line formed by separator lines or saddle connectors bifurcates into two distinct neutral lines. One bifurcated neutral line forms the wedge-shaped magnetotail whose neutral line moves earthward on the dusk side magnetotail, thus allowing the southward IMF to connect to the Earth's magnetic field. Another bifurcated neutral line preserves the old northward IMF topology on the dawn side magnetotail. They unify near the midnight meridian plane. On the dawn side magnetotail, saddle-connected three nulls form a magnetic "hole" or "path" that allows the southward IMF intruding into the magnetotail region to connect to the Earth's magnetic field. This transient topology appears just before the substorm onset and disappears at the onset, expanding the wedge-shaped neutral line on the dusk side magnetotail dawnward, completing the wedge-shaped neutral line to prevail fully in the magnetotail.

1. Introduction

In a three-dimensional (3D) magnetic field **B**, the solenoidal condition is $\nabla \cdot \mathbf{B} = 0$. Assuming those nulls, where the **B** field vanishes, are isolated. The flow behaviors near the nulls are determined by the eigenvalues of their **B** field Jacobians. Suppose all real parts of the eigenvalues of their Jacobians are non-zero, and the sum of three eigenvalues is zero. This implies that the real part of one eigenvalue has a different sign from the other two. Thus, the nulls in the 3D magnetic field are all saddle points, as shown in Figure 1a. As indicated in Figure 1a, B/Bs denotes the radial/spiral repelling nulls, while A/As denotes the radial/spiral attracting nulls. In the present report, we also refer to a null as CP (critical point).

Manuscript received 15 December 2023.

Peikun Xiong and Dongsheng Cai are with the University of Tsukuba, Ibaraki, Japan; e-mail: xiong@cavelab.cs.tsukuba.ac.jp, cai@cs.tsukuba.ac.jp.

Shigeru Fujita is with Research Organization of Information and Systems, Tokyo, Japan; e-mail: sfujita@ism.ac.jp.

Masakazu Watanabe and Takashi Tanaka are with Kyushu University, Fukuoka, Japan; e-mail: watanabe.masakazu.852@m.kyushu-u.ac.jp, takashi.tanaka.084@m.kyushu-u.ac.jp.

Near a null $\boldsymbol{x}_0$, two eigenvectors associated with negative (positive) real parts of eigenvalues span a two-dimensional (2D) (un)stable eigenspace $E^{(u)s}(\boldsymbol{x}_0)$. Here, "u" and "s" denote "unstable" and "stable," respectively, correlating to the magnetic field direction toward the null that is "attracting" and "repelling" behaviors toward the null. They are determined by the sign of the eigenvalues (negative for stable, positive for unstable). The 2D local (un)stable manifolds, $W_{loc}^{(u)s}(\boldsymbol{x}_0)$, tangent to $E^{(u)s}(\boldsymbol{x}_0)$, extend continuously from the nulls, forming a 2D separatrix, referred to as $W^{(u)s}(\boldsymbol{x}_0)$. The third eigenvector, whose eigenvalue has a different sign from the others spans the 1D (un)stable manifold $W_l^{(u)s}(\boldsymbol{x}_0)$. Usually, two or more nulls whose real part of eigenvalues have different signs can be connected by a saddle connector and form the saddle connection [1], as shown in Figure 1b. In the present study, we also use $\sum$ to represent the 2D manifold $W^{(u)s}(\boldsymbol{x}_0)$ and γ to represent the 1D manifold $W_l^{(u)s}(\boldsymbol{x}_0)$.

In the present study, we visualized the magnetospheric topologies in a near-Earth space based on the Magnetohydrodynamics (MHD)-simulation result reported by Tanaka et al. [3]. The simulation replicates a magnetospheric substorm triggered by a transition of the interplanetary magnetic field (IMF) from northward to southward orientation [4]. A substorm, also known as a magnetospheric or auroral substorm, represents a brief disturbance in the Earth's magnetosphere that causes energy to be released from the magnetotail and injected into the high latitude ionosphere (eg, see [5]). Substorms manifest through sudden changes in auroral emissions and alterations in magnetic fields, as measured by ground-based magnetometers, among other indicators. MHD-simulation studies by Honkonen et al. [6] investigated the magnetic topologies of large plasmoids in the magnetotail and discussed how these topologies form as a result of significant and rapid rotations of the IMF. Fryer et al. [7] investigated how the magnetosphere responds to the change of the By component of the magnetic field from $\pm$ 2 min in a northward IMF. They also discussed the influence of the "alpha-like" magnetotail topology and its impact on the IMF rotation. In the present report, we focused on visualizing the changes in magnetic field topologies detailed in the following just before the onset. These are referred to as bifurcations in mathematics caused by the brief disturbance generated only by the reversal of the IMF. Of note is the ongoing debate regarding the necessity of IMF reversal for substorm initiation. See reference [8] for further discussion.

During the substorm, the nulls are newly created and annihilated in near-Earth space, playing a crucial role in characterizing topological bifurcations according

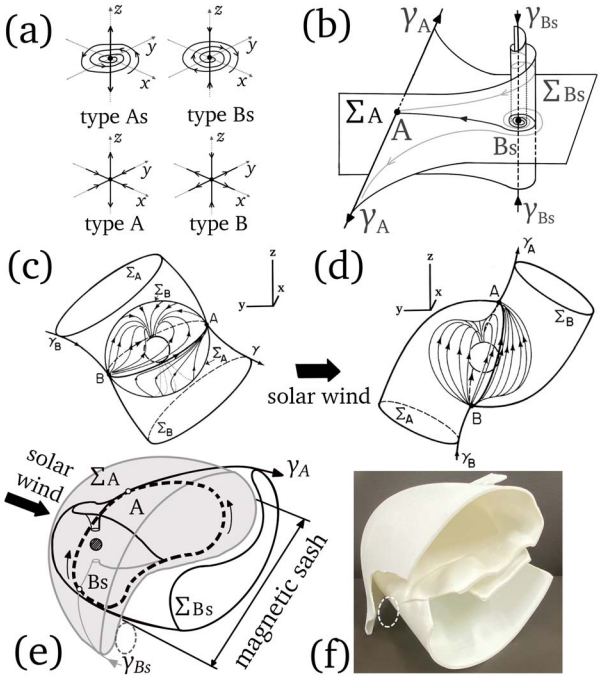

Figure 1. (a) A/As-type null is a radial/spiral attracting saddle point; B/Bs-type null is a radial/spiral repelling saddle point. (b) Saddle connection between A- and Bs-type nulls. The simplest schematic magnetospheric topologies in southward (c) and northward (d) IMF between A and B type nulls were originally illustrated by Lau and Finn [2]. (e) Schematic illustration from Figure 2. Neutral lines are illustrated in the bold dashed curves. (f) 3D printed topology of (e).

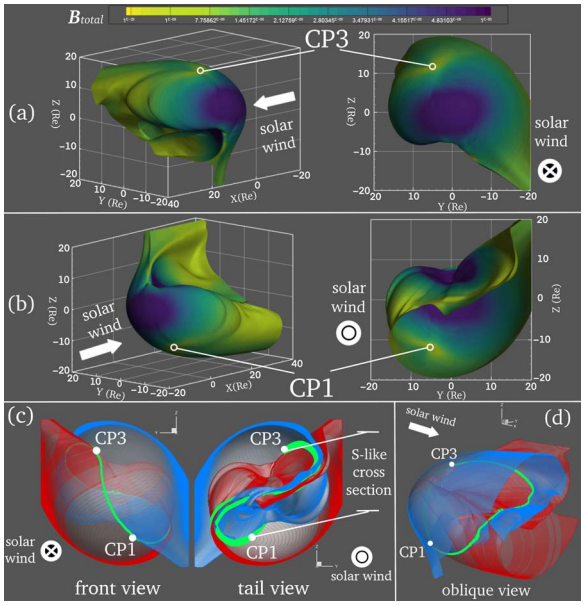

Figure 2. Global magnetospheric topology under northward IMF. Panel (a) and (b) are, respectively, from CP3 of $W^u(\boldsymbol{x}_{CP1})$ and CP1 of $W^s(\boldsymbol{x}_{CP3})$ with the surface color-coded with $\boldsymbol{B}_{total}$. Panel (c) and (d) are the saddle connection between $W^u(\boldsymbol{x}_{CP1})$ in red and $W^s(\boldsymbol{x}_{CP3})$ in blue with the cross-section or neutral lines or rings (bold green curves) in different views.

to vector field topology theory [9]. In the present report, we used a reliable numerical method, the geodesic level set method [10–12], to extract and visualize the 3D magnetospheric topologies from the nulls. The geodesic level set method is an iterative process that constructs a manifold by expanding from an initial set, using the eigenspace to define its starting geometry. Continuously solving a boundary value problem through the shooting method accurately determines new points on the manifold, maintaining a constant geodesic distance between them. Each iteration adds a new "band" to the surface, with the cumulative bands forming the full geodesic level set. For the details, please see [13].

2. 3D Magnetospheric Topologies in MHD

The MHD-simulation data were obtained from the REProduce Plasma Universe code [14]. The simulation began with a northward IMF (Bx = 0.0 nT, By = −4.3 nT, Bz = 4.3 nT), and turned into a southward (Bx = 0.0 nT, By = −4.3 nT, Bz = −4.3 nT). The input solar wind density—$Nsw = 5/cm^3$, speed $Vsw = 350Km/s$, and temperature $Tsw = 350,000K$—are maintained constant throughout the simulation [3]. We resample the original unequal-side-hexahedron grid from the results reported in [3] into the regular cubic grid data with the grid size 0.25 Re (Radius of the Earth). The detailed resampled conditions are stated in [13]. The geocentric solar-magnetospheric coordinate system is adopted, with the X, Y, and Z axes pointing tailward, dawnward, and northward, respectively.

2.1 3D Topology in Steady State Northward IMF

Based on the field topology theory, Lau and Finn [2] illustrated saddle-connected cylinder-like manifold pairs for both northward and southward IMFs, including the Earth's dipole, as shown in Figures 1c and 1d. This topology has never been visualized using a global MHD simulation or other simulation methods. For the first time, this study visualizes a pair of globally saddle-connected topologies corresponding to the topology described by Lau and Finn [2] between the null CP 1 and 3 located in the south and north, as displayed in Figure 2. We identified a total of five nulls, labeled CP 1 to 5, among which only CP 1 and 3 form the global topology of interest. The remaining nulls, contributing to local topologies, are deemed insignificant for the scope of this report and thus are not further discussed.

The global 2D unstable $W^u(\boldsymbol{x}_{CP1})$ and stable $W^s(\boldsymbol{x}_{CP3})$ manifolds are visualized in Figures 2a and 2b. They have a cylinder-like manifold, respectively, with one end diverging into the northern and southern magnetotail, and the other end converging into the south and north terrestrial poles. The colors on the manifolds in Figures 2a and 2b represent the magnetic field intensity $\boldsymbol{B}_{total}$. Please note $W^u(\boldsymbol{x}_{CP1})$ and $W^s(\boldsymbol{x}_{CP3})$ do not diverge toward infinity north and south, instead, they diverge into the tail to form the magnetotail magnetosphere. The magnetic

field is relatively weak near two light-yellow regions near the null CP 1 and 3. The magnetic field is relatively stronger near the day-side bow shock, subsolar point, and near the north and south poles.

Figures 2c and 2d show a saddle connection between $W^s(\boldsymbol{x}_{CP3})$ and $W^u(\boldsymbol{x}_{CP1})$. In Figures 2c and 2d, $W^u(\boldsymbol{x}_{CP1})$ and $W^s(\boldsymbol{x}_{CP3})$ are, respectively, shown in red and blue meshes. The intersection between $W^u(\boldsymbol{x}_{CP1})$ and $W^s(\boldsymbol{x}_{CP3})$ forms a ring consisting of two "neutral lines." This neutral ring is shown in Figures 2c and 2d in bold green. Both neutral lines start from CP 1 in the south, flow diagonally along the day and night sides of the magnetosphere, respectively, and connect to CP 3 in the north. In this visualization, the global magnetospheric topology can only be identified by this saddle connection between CP 1 and 3. The narrow and sandwiched pathway or slit (the S-like cross-section) located between $W^u(\boldsymbol{x}_{CP1})$ and $W^s(\boldsymbol{x}_{CP3})$ in the tail forms the weak magnetic field path that corresponds to the magnetic sash [15]. This sandwiched path near the equatorial plane also locationally corresponds to the plasma sheet in the magnetotail. In Figure 1e, the Σ_B and Σ_A surfaces correspond, respectively, to $W^u(\boldsymbol{x}_{CP1})$ and $W^s(\boldsymbol{x}_{CP3})$.

Figures 1e and 1f are schematically illustrated and 3D printed topologies of Figure 2d. They are also topologically equivalent to that in Figure 1d. Unlike the topology in Lau and Finn [2, fig. 1d], one end of both cylinder-like manifolds Σ_A and Σ_B do not extend, respectively, toward infinity north and south but extend tailward from the south dusk and north dawn. They cross each other on the nightside. mainly near the equatorial plane, forming the S-like cross-section, as shown in Figures 1e and 1f and Figures 2c and 2d.

Furthermore, the S-like slit sandwiched between $W^u(\boldsymbol{x}_{CP1})$ and $W^s(\boldsymbol{x}_{CP3})$ tailward near the equator plane corresponds to the plasma sheet in location. The relation between the plasma sheet in the magnetotail and the part of this S-like slit sandwiched between these two manifolds $W^u(\boldsymbol{x}_{CP1})$ and $W^s(\boldsymbol{x}_{CP3})$ needs further study to determine if they are identical or not. In the present paper, we mainly focused on their topologies in time.

2.2 3D Topology Just Before Substorm Onset

Next, we visualize the 3D magnetospheric topology 3.34 min before the substorm onset after the southward IMF turning, as visualized in Figure 3. The onset time is identified when the cross-tail current flowing through the plasma sheet is disrupted, and a high-speed plasma flow is generated; for details, please see [3]. Currently, 7 of 12 identified nulls are integral to the global topology, all situated along the neutral line. In the present paper, "global topology" refers to the comprehensive magnetospheric topology, with all relevant nulls positioned along the neutral line. The blue cylinder-like manifold extending northward consists of the 2D stable manifolds constructed from A or As-type CP 6 (As), 10 (As), and 11(A), and the red cylinder-like manifold extending southward consists of the 2D

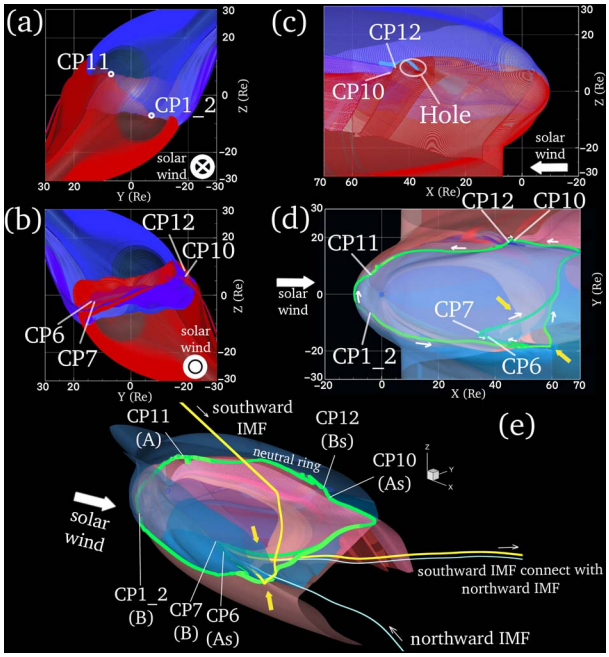

Figure 3. The 3D global magnetospheric topology 3.34 min before the substorm onset. The front (a), back (b), dawnside (c), above north (d) and back and oblique (e) view of a saddle-connected topology mainly between $W^u(\boldsymbol{x}_{CP1\_2,7,12})$ in redish and $W^s(\boldsymbol{x}_{CP6,10,11})$ in bluish. The neutral lines are shown in bold green.

unstable manifolds constructed from B or Bs-type CP 1 (B), 2 (B), 7 (B), and 12 (Bs). Here, CP 1 and 2 are located very closely, yet their distance is still larger than the grid size, and topologically, their eigenspaces are considered to be identical [16]. Here, an A/As-type CP refers to a radial/spiral attracting saddle point, whereas a B/Bs-type CP refers to a radial/spiral repelling saddle point, as indicated in Figure 1a. The saddle-connected lines between each pair of positive (B/Bs) and negative (A/As) nulls form the so-called neutral ring (bold green curves) encircling the terrestrial magnetosphere. At this time, the magnetotail is stretched to its maximum size and is about to release the plasmoid.

The neutral ring in the dusk side tail is both bifurcated and unified to form the wedge-shaped line as evidenced in the region indicated by bold yellow arrows in Figure 3. This is the saddle connection composed of more than three nulls. Figure 3 shows that CP 6, 10, and 11, which span the blue manifolds, and CP 1_2, 7, and 12, which span the red manifolds, are saddle connected and comprise the main part of the global topology of the magnetosphere. In addition to this saddle connection, Figure 3b shows a newly generated saddle connection between CP6 and 7, constituting the bifurcated and unified wedge-shaped neutral lines shown in Figures 3d and 3e.

Both the new wedge-shaped neutral line at the dusk side of a half magnetotail region and the old neutral line before the IMF turning unification near the midnight meridian plane. This indicates the coexistence of the old and new magnetosphere generated by the

IMF turning in the dusk side magnetotail region. This can also be evidenced by one light blue northward IMF line and one yellow southward IMF line that penetrates this wedge-shaped neutral line area and both connect to the northward IMF, as shown in Figure 3e.

In total, 7 nulls are connected along the neutral rings and forming the magnetospheric global topology, except the dusk side magnetotail. It is essentially identical to the schematic illustration of the Earth's magnetospheric topology in a southward IMF by Lau and Finn [2] shown in Figure 1c. However, it also partially preserves the old magnetospheric structure, as observed by the asymmetric neutral line in the magnetotail.

3. Asymmetries in 3D Magnetospheric Topology

3.1 Asymmetry in Steady State Northward IMF

In section 2.1, we discussed the existence of the narrow slit sandwiched between the north and south magnetospheric lobes $W^u(\boldsymbol{x}_{CP1})$ and $W^s(\boldsymbol{x}_{CP3})$. It corresponds to the magnetic sash and also corresponds to the plasma sheet near the equator plane in location. However, as shown in Figures 1e and 1f and Figures 2c and 2d, a strong asymmetry exists between the dusk and dawn side flank of the magnetosphere. The S-shaped slit is widely open at the dusk flank of the magnetosphere, as indicated by the dashed ellipse in Figure 1e. The width can be more than 6∼7 Re (Radius of Earth). On the other hand, the width of the S-shaped slit at the dawn flank of the magnetosphere is about 2∼3 Re. We expect the new IMF can use this wide-open path at the dusk flank of the magnetosphere to penetrate and reconnect partly with the separatrices $W^u(\boldsymbol{x}_{CP1})$ and $W^s(\boldsymbol{x}_{CP3})$ that sandwich the S-shaped slit near the neutral line and equator plane.

We also expect this causes the asymmetric magnetospheric topology at the dusk side magnetotail, as evidenced by the bifurcated and unified neutral lines in Figures 3d and 3e. During and after the southward IMF turning, the outer separatrices can easily reconnect with the new IMF. However, near the equatorial plane at the magnetotail, the separatrices of north and south magnetospheric lobes are antiparallel. The hot plasma sheet can prevent those separatrices from reconnecting with the new IMF by eing sandwiched between them near the midnight equatorial plane.

3.2 Magnetic "Hole" at Dawn Side Flank of Southward Lobe Magnetosphere

Furthermore, the asymmetric topological structure at the magnetotail must be resolved to generate a new topology for the southward IMF as schematically illustrated in Lau and Finn [2, fig. 1c], possibly during the substorm onset. A wide magnetic slit between $W^u(\boldsymbol{x}_{CP1})$ and $W^s(\boldsymbol{x}_{CP3})$, is not observed at the dawn-side flank of the southward magnetospheric lobe in the steady state northward IMF. However, near CP12 along

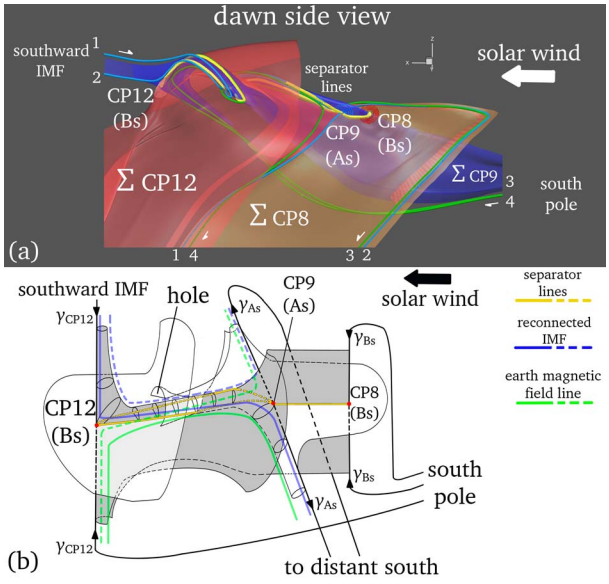

Figure 4. (a) Visualized Bs-As-Bs saddle connection on the dawn side south lobe just before the onset. (b) Schematic figure of (a).

the null-null lines just before the onset, we find a magnetic "hole" generated by three null saddle connections, as shown in Figure 4. They are Bs (CP12, located along the neutral ring)-As (CP9)-Bs (CP8) type saddle connection. The null CP9 and CP8 indicated in Figure 4 (on the right side) are saddle connected, located near and inside the magnetosphere, and do not belong to the neutral ring. One 2D stable manifold in blue from the CP9 spirals and expands to CP8. This half manifold also expands further and attracts into the Earth's dipole.

This CP9 (As-type) null is also saddle connected with CP12 (Bs-type) with two bifurcated saddle-connecting lines or the separator lines (yellow curves), as shown in Figures 4a and 4b. Here, another half 2D stable manifold from CP9 spirals and expands along the 1D manifold γ_{CP12} on the southward lobe, which is indicated as the tiny light blue tube manifold shown in Figure 3c. This half 2D stable manifold also extends and penetrates further toward the magnetotail region. This CP12-CP9-CP8 saddle connection, as visualized in Figure 4, forms a complicated "hole" or "tube-like" magnetic structure. Through this "hole," the magnetic field lines 1 and 2 in blue, as shown in Figures 4a and 4b, originated from the southward IMF and can connect to infinity south, passing through the magnetotail region.

Table 1 lists Bx, By, and Bz, as well as determinants of the **B** field Jacobian sampled along one of the saddle-connecting lines between CP12 and CP9. The magnetic field component values at the null CP12 and CP9 are small enough to be regarded as zeros. Excluding the null points, the magnetic field components Bx, By, and Bz at sampling points P1∼P6 are significant, yet they are a factor of 10^{-1} smaller than the ambient magnetic field values near this "hole" path, which are not specified here. Furthermore, the determinants of the

Table 1. The magnetic field and its determinant of the **B** field Jacobian at the points CP 12, P1∼6, and CP 9.

	Bx	By	Bz	Determinant of **B** field Jacobian
CP12 (Bs)	1.13^{E-26}	3.23^{E-27}	-6.46^{E-27}	-2.74^{E-30}
P1	-1.65^{E-09}	-8.89^{E-11}	9.00^{E-10}	-4.82^{E-29}
P2	1.54^{E-08}	-1.34^{E-09}	4.06^{E-09}	1.06^{E-29}
P3	-9.88^{E-11}	-2.84^{E-10}	-1.59^{E-10}	2.32^{E-30}
P4	-2.44^{E-09}	-6.44^{E-10}	5.97^{E-10}	-2.85^{E-30}
P5	-3.78^{E-09}	1.41^{E-10}	-6.68^{E-10}	6.34^{E-30}
P6	-1.94^{E-09}	-2.23^{E-10}	-6.77^{E-10}	-2.56^{E-30}
CP9 (As)	-6.46^{E-27}	8.08^{E-28}	-1.29^{E-26}	9.88^{E-29}

magnetic field at these points, although not detailed here, are also significantly smaller when compared to those in the surrounding ambient magnetic field.

The sampling points P1-P6 are along one of the saddle-connected paths between CP12 (Bs) and CP9 (As).

The magnetic field can be Taylor expanded as $\mathbf{B} = \mathbf{B}_0 + \frac{\partial B_i}{\partial x_j} x_j + \frac{1}{2}\frac{\partial^2 B_i}{\partial x_j \partial x_k} x_j x_k + \mathbf{O}$ (3). Those small values of $\mathbf{B}_0$ field components and the almost zero values of the determinant of Jacobian $\frac{\partial B_i}{\partial x_j}$ along this "hole" indicate that the terms higher than the first order inside this "hole" are not negligible and have to be considered. Thus, the magnetic "hole" observed here cannot be treated by the linear vector field theory we discussed in Section 1. The null classifications in Figure 1 are no longer applicable. This magnetic "hole" structure is nonlinear, and higher-order terms must be considered. The nonlinearity can also be evidenced by the double saddle connectors.

The significant point we have to stress here is that this "hole" can expand toward the magnetotail region near the equator plane as time advances toward the substorm onset. Finally, the wedge-shaped neutral curve at the dusk side is expanded dawnward to prevail in the whole magnetotail region, and then bifurcated and unified double neutral curves are combined to be one wedge-shaped neutral curve. Then, the substorm onset starts. The details and mechanisms of these changes in topologies or "bifurcations" are still under intensive investigation.

4. Conclusions

The dynamics of the magnetospheric substorm onset is a highly complex physical phenomenon. The present report uses the geodesic level set method to visualize the 3D magnetospheric topologies in a 3D global MHD simulation before the substorm onset. For the first time, we visualize the realistic terrestrial magnetic topologies during the steady state northward IMF and growth phase (pre-onset) of the substorm.

In steady-state conditions with a northward IMF orientation, as depicted in Figure 2, the visualized terrestrial magnetic topology—comprising the north and south lobe manifolds, $W^u(\boldsymbol{x}_{CP1})$ and $W^s(\boldsymbol{x}_{CP3})$, respectively—aligns closely with the magnetospheric magnetopause boundary as measured by satellites and predicted by various global MHD simulations. Realistic neutral rings are obtained by taking a cross-section between the two global manifolds (ie, the south and north lobe manifold $W^u(\boldsymbol{x}_{CP1})$ and $W^s(\boldsymbol{x}_{CP3})$ generated from the north and the south nulls). We find that tailward of the neutral line, the north and south magnetospheric lobe manifold $W^u(\boldsymbol{x}_{CP1})$ and $W^s(\boldsymbol{x}_{CP3})$ do not extend toward infinity north and south but extend toward the distant tail and form the sandwiched path that locationally corresponds to the magnetic sash. This narrow path or slit sandwiched between these two manifolds is open and can connect to the solar wind.

Asymmetric terrestrial magnetospheric topology is visualized in the substorm growth phase at −3.34 min before the substorm onset. In the magnetotail region, the bifurcated and unified wedge-shaped neutral curves are generated at the dusk side of the magnetotail, which evidences the coexistence of the old and new magnetospheric topologies. At the dawnside flank of the magnetospheric lobe, a magnetic "hole" structure connecting the southward IMF to the north pole magnetic field is transiently formed by the CP12(Bs)-CP9(As)-CP8(Bs) saddle connection. As time advances, this "hole" or "tube" briefly penetrates the dawn side magnetic lobe, allowing outer IMF field lines to intrude into the plasma sheet region. This allows half of the dawn side neutral line to move significantly toward the Earth. Thus, one symmetrical wedge-shaped neutral line is formed, and the substorm onset starts.

Our work is still preliminary and is the first attempt to visualize the magnetospheric topology at different times, with the purpose of observing the topological change during the substorm.

5. References

1. H. Theisel, T. Weinkauf, H. C. Hege, and H. P. Seidel, "Saddle Connectors-An Approach to Visualizing the Topological Skeleton of Complex 3D Vector Vields," IEEE Visualization, Seattle, WA, USA, October 19–24, 2003, pp. 225-232.
2. Y. T. Lau and J. M. Finn, "Three-Dimensional Kinematic Reconnection in the Presence of Field Nulls and Closed Field Lines," *The Astrophysical Journal*, **350**, 2, February 1990, pp. 672-691.
3. T. Tanaka, Y. Ebihara, M. Watanabe, M. Den, S. Fujita, T. Kikuchi, et al., "Development of Magnetic Topology During the Growth Phase of the Substorm Inducing the Onset of the Near-Earth Neutral Line," *Journal of Geophysical Research: Space Physics*, **124**, 7, July 2019, pp. 5158-5183.

4. E. Priest and T. Forbes, *Magnetic Reconnection: MHD Theory and Applications*. Cambridge, UK, Cambridge University Press, 2000.
5. M. Kivelson and C. Russell, *Introduction to Space Physics*, Cambridge, UK, Cambridge University Press. 1995.
6. I. Honkonen, M. Palmroth, T. I. Pulkkinen, P. Janhunen, and A. Aikio, "On Large Plasmoid Formation in a Global Magnetohydrodynamic Simulation," *Annales Geophysicae*, **29**, 1, January 2011, pp. 167-179.
7. L. J. Fryer, R. C. Fear, I. L. Gingell, J. C. Coxon, M. Palmroth, et al., "3D GUMICS Simulations of Northward IMF Magnetotail Structure," *Journal of Geophysical Research: Space Physics*, **128**, 8, July 2003, p. e2023JA031317.
8. S. K. Morley and M. P. Freeman, "On the Association Between Northward Turnings of the Interplanetary Magnetic Field and Substorm Onsets," *Geophysical Research Letters*, **34**, 8, April 2007.
9. E. R. Priest, D. P. Lonie, and V. S. Titov, "Bifurcations of Magnetic Topology by the Creation or Annihilation of Null Points," *Journal of Plasma Physics*, **56**, 3, March 1996, pp. 507-530.
10. H. M. Osinga and B. Krauskopf, "Visualizing the Structure of Chaos in the Lorenz System," *Computers & Graphics*, **26**, 5, October 2002, pp. 815-823.
11. B. Krauskopf and H. M. Osinga, "Computing Geodesic Level Sets on Global (Un)stable Manifolds of Vector Fields," *SIAM Journal on Applied Dynamical Systems*, **2**, 4, 2003, pp. 546-569.
12. B. Krauskopf and H. Osinga, "Two-Dimensional Global Manifolds of Vector Fields," *Chaos: An Interdisciplinary Journal of Nonlinear Science*, **9**, 3, September, 1999, pp. 768-774.
13. P. Xiong, S. Fujita, M. Watanabe, T. Tanaka, and D. Cai, "Identifying and Visualizing Terrestrial Magnetospheric Topology using Geodesic Level Set Method," Computer Graphics Forum, **43**, 1, November 2023, p. e14994.
14. T. Tanaka, Y. Ebihara, M. Watanabe, M. Den, S. Fujita, et al., "Global Simulation Study for the Time Sequence of Events Leading to the Substorm Onset," *Journal of Geophysical Research: Space Physics*, **122**, 6, May 2017, pp. 6210-6239.
15. W. W. White, G. L. Siscoe, G. M. Erickson, Z. Kaymaz, N. C. Maynard, et al., "The Magnetospheric Sash and the Cross-Tail S," *Geophysical Research Letters*, **25**, 10, May 1998, pp. 1605-1608.
16. S. H. Strogatz, *Nonlinear Dynamics and Chaos: With Applications to Physics, Biology, Chemistry, and Engineering*, Boca Raton, FL, CRC Press, 2018.